Determining multi-scale controls on river temperature: a time series approach

Michael Vlah

March 29, 2017

Summary:
5 data sources; watershed delineation; 2 DFAs: m=1:15, 7 covariate combinations, 4 err. struc., 2 seasonality models; TMB; parallel computing; Bayesian change/time

Abstract

Temperature is among the most important determinants of riverine biodiversity and health. It is therefore a primary freshwater management concern, particularly where cold-water fish are of high ecological, recreational, and commercial value. However, river temperature in the Puget Sound watershed of the Northwestern U.S.A. is affected by a great diversity of drivers at multiple spatial and temporal scales, and little is known of their interactions. We used dynamic factor analysis, a multivariate time-series technique, to examine relationships among these drivers, synthesizing long-term climate and fine-scale landcover data. We found that primarily rain-fed rivers experience large seasonal temperature fluctuations, which closely track atmospheric temperature, while snow-fed rivers tend to be weakly, and in some cases inversely, coupled with such fluctuations. Among watersheds, groundwater influx, land slope, and discharge further augment or dampen these relationships. Our results suggest the temperature of high-elevation rivers, absent the influence of ice, should be highly variable, and that glacially fed streams stand to see the largest changes in temperature regime under proposed climate scenarios.

Introduction

The ecological condition of a stream or river, the life it supports, and the goods and services it provides, are influenced by the timing and magnitude of seasonal changes in water temperature. Temperature is a chief consideration in the management of fisheries, as it affects species distribution (Boisneau et al., 2008), growth and reproduction (McCullough, 1999), and migration timing (Boscarino et al., 2007). In particular, In the Puget Sound watershed of the American Pacific Northwest, several salmonid species spawn, migrate, and emerge only within the bounds of a few degrees Celsius, and thrive under even greater temperature constraints (Carter, 2005). As a result, the success of commercial and recreational fisheries that depend on the region's riverine habitat rests on many precarious factors.

River networks, being fractal in structure, are naturally governed by environmental processes at multiple scales. Seasonal variation in water temperature in rivers of the Pacific Northwest is a function of the surrounding air, as well as precipitation and snowmelt (Eldridge, 1967). These drivers may in turn be mediated or supplemented by several aspects of watershed morphology at smaller scales, including slope, elevation, and geology (Poole and Berman, 2001; Lisi et al., 2013). Taken together, this hierarchical system complicates fishery management, as the temperature regime of one river may be the direct product of climate, while that of another may depend more on within-watershed conditions.

Adding to this picture, flow regimes across rivers of the Puget Sound watershed vary with latitude and elevation (Reidy Liermann et al., 2012; Mauger et al., 2015), and can be classified broadly into three categories by flow source and hydrograph shape. Rain-dominated (RD) rivers receive little or no input from snowmelt, and thus peak in discharge during the rainy season, usually between October and February. Snow-dominated (SD) rivers instead see peak flow during spring snowmelt, often in April, May, or June. Between these extremes lies a third class of rain-and-snow-driven (RS) rivers, which have appreciable peaks at both times.

Effective management plans must therefore integrate a diversity of factors across space and time in order to determine which rivers and watersheds are likely to see consequential changes under projected climate and land use scenarios for the Pacific Northwest (Mote and Salathe, 2010; Radeloff et al., 2012). However, the understanding required to do so is limited by knowledge of relationships among temperature drivers at scale.

We sought to identify streams in the Puget Sound region whose temperatures fluctuate closely with regional trends in air temperature, precipitation, and snowmelt, and those that depart from regional patterns. Our second aim was to identify watershed features that correlate with such departures, and thus provide a nuanced basis for predicting impacts of water temperature on aquatic biodiversity and fishery health. We hypothesized that water temperature would track air temperature most closely in RD rivers (Ward, 1985; Garner et al., 2014). We expected deviations from this relationship to correlate best with cold-water influx from snow and ice melt (Lisi et al., 2015) and with factors

affecting heat capacity of water, including discharge (volume over time) and watershed slope (which relates to turbulence, surface area, and mixing; van Vliet et al. 2013).

Methods

Water and climate data

We investigated climate and landscape controls on water temperature and discharge, as separate response variables, from 1978 to 2015. Monthly time series of water temperature were obtained for 24 river sites via the Washington Department of Ecology's River and Stream Water Quality Monitoring program (Von Prause, 2017). These sites represent 19 nonnested watersheds across 9 counties, and range from 4 to 775 m in elevation. For at least one site at each river, monthly discharge time series were also available, either from the same location as one of the temperature monitoring sites, or from within 30 km on the same major reach. Discharge data were aggregated by monthly mean from the USGS National Water Information System database (USGS, 2017).

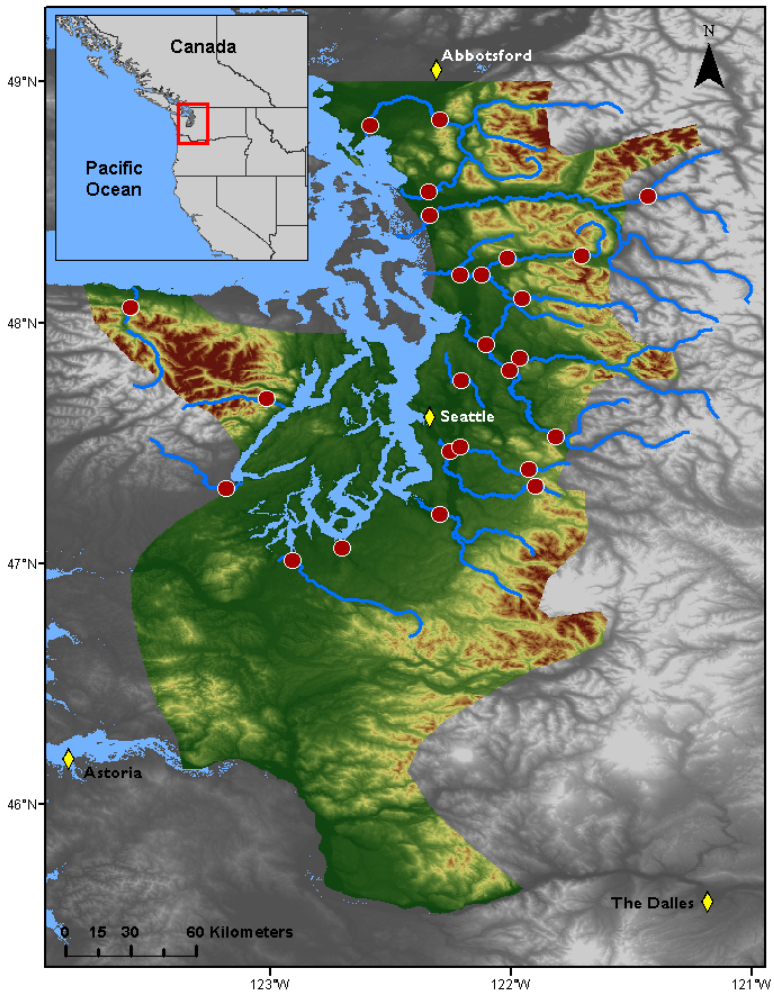

Figure 1 Site locations (red points) in relation to combined Washington State Climate Divisions 3 and 4 (colored topography), the region across which climate data were aggregated.

Potential climatic predictors of water temperature and discharge included mean and max air temperature (°C), total precipitation (cm), snowmelt (cm), and hydrological drought (Palmer Hydrological Drought Index), averaged by month across the response variable time series. All but snowmelt were available through the U.S. Climate Divisional Dataset, developed by the National Cen-

ters for Environmental Information (NCEI; NOAA 2017). We acquired climatic predictor data grouped by Washington State climate division, and all but two of our sites fell within divisions 3 (Puget Sound Lowland) and 4 (East Olympic/-Cascade Foothills; see Fig. 1). We therefore aggregated these data by monthly mean across the two regions (after verifying their post-standardization similarity), resulting in a single dataset of four climatic predictor variables. A snowmelt time series was then added to this dataset, using monthly mean records from six SNOTEL sites (Bumping Ridge, Elbow Lake, Mount Crag, Park Creek Ridge, Stevens Pass, White Pass) listed by the USDA's Natural Resources Conservation Service; USDA 2017. We calculated monthly snowmelt for each site as the absolute value of negative differences in cumulative snow water equivalent from each month to the next. The snowmelt time series was assigned zeros for any positive differences (accumulations).

Time series analysis

Response time series were modeled using dynamic factor analysis (DFA; Zuur et al. 2003b), a multivariate technique that can be thought of as an analog to principal component analysis in the time domain. In DFA, response time series are fit with a linear combination of shared, random-walk trends (usually many fewer than the total number of response series), predictors (which can have unique effects on each response series), and random error. We chose DFA over a traditional multivariate state space approach for two reasons. First, it provides advantages in computational efficiency, as a small number of shared trends often adequately capture variation across dozens of responses, and at much lower parameter cost (Zuur et al., 2003a). Second, in terms of identifying what drives the shared trends, having fewer of them allows for greater inferential parsimony. Being a multivariate technique, DFA also provides an advantage over univariate alternatives in that covariance structure among responses can be specified and compared. All models were fit using maximum likelihood estimation by automatic differentiation, with Template Model Builder software (Kristensen et al., 2015), which we called using package TMB in R (R Core Team, 2017; Kristensen et al., 2016).

DFA takes the following form:

$$\mathbf{x}_t = \mathbf{x}_{t-1} + \mathbf{w}_t, \text{ where } \mathbf{w}_t \sim \text{MVN}(0, \mathbf{Q}) \tag{1}$$

$$\mathbf{y}_t = \mathbf{Z}\mathbf{x}_t + \mathbf{D}\mathbf{d}_t + \mathbf{v}_t, \text{ where } \mathbf{v}_t \sim \text{MVN}(0, \mathbf{R}) \tag{2}$$

$$\mathbf{x}_0 \sim \text{MVN}(0, \mathbf{\Lambda}) \tag{3}$$

At time step t, the $m \times 1$ vector of shared trends ($\mathbf{x}$) is a function of $\mathbf{x}$ in the previous step, plus normal error ($\mathbf{w}$; $m \times 1$; Eq. 1). This is the definition of a random walk. The $n \times 1$ response vector ($\mathbf{y}$) at time t is a function of the shared trends and their factor loadings ($\mathbf{Z}$; $n \times m$), covariates ($\mathbf{d}$; $q \times 1$) and their river-specific effects ($\mathbf{D}$; $n \times q$), and a second normal error term ($\mathbf{v}$; $n \times 1$; Eq. 2). $\mathbf{R}$ and $\mathbf{Q}$ are variance-covariance matrices of order m, and $\mathbf{Q}$ is

set to identity for model identifiability (Harvey, 1990). The initial state of the shared trend vector ($\boldsymbol{x}_0$) is multivariate-normally distributed with a mean of zero and a diagonal variance-covariance matrix with large variance (e.g. 5; Eq. 3). Response and predictor data were standardized to facilitate comparison of effect sizes and avoid error inflation.

Because we were interested in isolating the effects of climatic predictors on river temperature and discharge, we used a fixed factor to account for recurring seasonal variation not related to the predictors, with one factor level for each month. This factor was incorporated into the covariate matrix ($\mathbf{d}$). Thus, the coefficient in $\mathbf{D}$ relating, say, precipitation (predictor) and water temperature (response), represents the effect size of the former on the latter. In other words, it is the change in water temperature accompanying a unit change in precipitation across the whole time series. We call this relationship "coupling." We were also interested in coupling by month for $\mathrm{T_{air}}$, which required that it be arranged as twelve separate, monthly time series. Concretely,

$$
\mathbf{d} = \begin{array}{c} \\ 1 \\ 2 \\ 3 \\ \\ 12 \\ 13 \\ 14 \\ 15 \\ 16 \\ 17 \\ \\ 26 \end{array}
\begin{array}{c}
\begin{array}{ccccc} \mathrm{Jan}_{1978} & \mathrm{Feb}_{1978} & \mathrm{Mar}_{1978} & \cdots & \mathrm{Dec}_{2015} \end{array} \\
\left(\begin{array}{ccccc}
1 & 0 & 0 & \cdots & 0 \\
0 & 1 & 0 & \cdots & 0 \\
0 & 0 & 1 & \cdots & 0 \\
\vdots & \vdots & \vdots & \ddots & \vdots \\
0 & 0 & 0 & \cdots & 1 \\
precip_1 & precip_2 & precip_3 & \cdots & precip_T \\
snowmelt_1 & snowmelt_2 & snowmelt_3 & \cdots & snowmelt_T \\
air_1 & 0 & 0 & \cdots & 0 \\
0 & air_2 & 0 & \cdots & 0 \\
0 & 0 & air_3 & \cdots & 0 \\
\vdots & \vdots & \vdots & \ddots & \vdots \\
0 & 0 & 0 & \cdots & air_T
\end{array}\right)
\end{array}
$$

is the covariate matrix structure necessary to account for seasonal variation of unknown origin (rows 1-12), and the effects of precipitation (row 13) and snowmelt (row 14), while also yielding the effect of air temperature by month (rows 15-26) on the response ($\mathbf{y}$; Eq. 2). This is the covariate structure of the model we used for subsequent analyses, not including those described in Figure 5d-e, and Appendix B.

Additional, non seasonal variation due to unknown factors manifests in the shared trends, and a portion of any residual variation is absorbed by error matrix $\mathbf{v}$. We fit models using four unique error structures ($\mathbf{R}$), to allow for multiple suites of unknown drivers affecting rivers. We included shared variance with zero covariance, individual variance with zero covariance, shared variance with shared covariance, and individual variance with individual covariance. Details on these structures and their implications can be found in (Holmes et al., 2012). The best models for water temperature and discharge were determined via AIC.

However, negligible likelihood improvements can be inflated when multiplied by thousands of data points, undermining common rules of thumb for admitting additional parameters under AIC (Burnham and Anderson, 2003). Thus, we had reason to doubt that the "most parsimonious" model according to AIC alone was any better than a much simpler alternative. To manage this, we required that each additional trend, covariate, or seasonal structure improve the median coefficient of determination (R^2) by at least 1% in order to justify accepting its attendant complexity.

Landscape predictors and post-hoc regression

For post-hoc analyses, monitoring sites were separated into three classes based on relative areal coverage of perennial ice and/snow (hereinafter "% glaciation") and mean elevation across their watersheds. The three classes are loosely based on the classification scheme and language of the Climate Impacts Group at the University of Washington (Mauger et al., 2015), and are here delineated according to Table 1.

Table 1 Watershed classification scheme

Classification	Abb.	Glaciation (%)	Mean elev. (m)
Rain-dominated	RD	< 0.7	< 600
Rain-and-snow	RS	< 0.7	≥ 600
Snow-dominated	SD	≥ 0.7	-

After model selection, climatic predictor effect sizes (**D**; Eq. 2) for each river were back-transformed to their original scales and regressed against landscape predictors in order to identify possible watershed-scale controls on coupling. To achieve this, we amassed an additional dataset of landscape features. These were collected individually for each of the watersheds corresponding to our 24 river sites, using the EPA's StreamCat (stream-catchment) data library (Hill et al., 2016) and the National Hydrography Dataset (NHDPlusV2; McKay et al. 2012). Each site was mapped to an individual river reach, defined as a segment bounded on each end by a stream or river source, confluence, or mouth. The region contributing flow to this reach (its watershed) was then fetched, along with selected areal data, from the NHDPlusV2 database. Landscape attributes used as predictors were aggregated by watershed mean where applicable, and include elevation (m), total area (km^2), base flow index, soil permeability (cm hr^{-1}), water table depth (cm), bedrock depth (cm), Base Flow Index (BFI; %), runoff (mm mo^{-1}), percent perennial ice and snow coverage (National Land Cover Database [NLDC] 2006 and 2011 average), riparian population density (people km^{-2} within 100m of streams; 2010 census), riparian road density (km km^{-2}; 2010 census), and percent riparian urban land (NLCD 2011). Monitoring site elevation (m) and presence of upstream dams (as full/partial/no damming of upstream mainstem and major tributaries) were also included. Finally, we calculated area above 1000 m (as % watershed area), mean slope (% rise), and

mean aspect (degree) by delineating and summarizing watersheds from a digital elevation model in ArcMap v. 10.4 (ArcMap, 2016).

An additional set of post-hoc regressions was performed using factor loadings on shared trends ($\mathbf{Z}$; Eq.2) as dependent variables, with landscape predictors again as independent variables. Loadings represent the degree to which each river's temperature fluctuates with the anonymous force driving the corresponding shared trend. A landscape feature that varies in proportion to these loadings is therefore likely to be a mediator of the anonymous force, if not the force itself. To facilitate inference by way of the shared trends, we made three simplifications to the model. We removed the monthly factor and the snowmelt predictor from the covariate matrix ($\mathbf{d}$, rows 1-12 and 14), so that the trends would be free to express seasonal and elevational variation. Then, we limited the number of trends to between one and three, to avoid "trend specialization." in other words, we optimized the trends for flexibility while concentrating their explanatory power. Additionally, we summarized the landscape predictors with principal coordinates analysis, as a way to conceptually "group" them by correlation. We used the Gower dissimilarity coefficient (Gower's distance) to account for association among both continuous and nominal variables (Gower, 1966).

Results

Mean monthly temperature trends for the three river classes, aggregated across all 38 years of data, deviated by a minimum of 1.0°C in December, and a maximum of 3.9°C in July (Fig. 2). SD rivers remained approximately two degrees colder than their RS counterparts through mid-late summer, and 3-4 degrees colder than RD throughout spring and summer. RD rivers were consistently warmest throughout the year. In January, RS reached a minimum of 4.4°C, and did not significantly differ from SD (Student's t: $p < 0.01, F = 11.9$). RD only attained a minimum of 5.6°C. RS reached a peak summer temperature of 16.9°C in July, while RS and SD followed in August with peak temperatures of 15.5 and 13.5°C, respectively.

Meanwhile, the amplitude of T_{air} oscillation exceeded that of any river class, dipping below T_{water} in autumn to a minimum of 3.2°C in December, and rising above RS and SD in March to an August maximum of 17.4°C. T_{air} did not overtake RD T_{water} until August, by which time the latter had begun to decline.

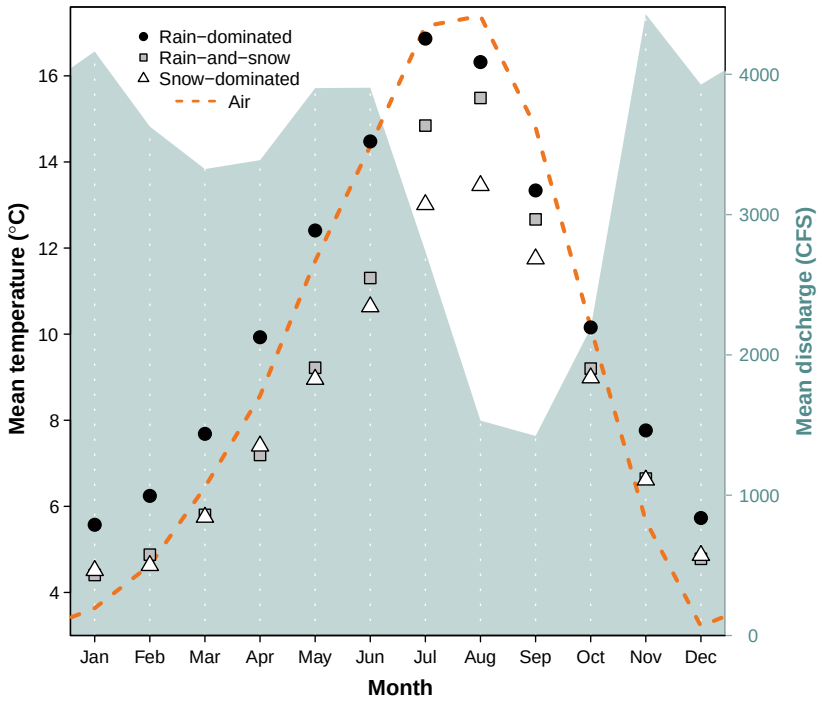

Figure 2 Monthly mean T_{water} by river class, and T_{air} and Q across classes, from 1978 to 2015. All depicted series represent discrete data.

The combined hydrograph of all rivers revealed two primary peaks, one beginning in late spring and the other extending from late fall to early winter, with a prominent trough in late summer. Spring peak discharge coincided noticeably with a separation in water temperature between SD and RS, while the summer trough coincided with separation of RD and T_{air}. On average, November marked both the autumn peak in discharge and the point at which T_{air} fell below T_{water}.

There was also an apparent divergence in slope between RD and all snow-influenced rivers, beginning in early spring and culminating in June. Between June and July, RS and SD saw a large jump in temperature, which coincided with the decline in snowmelt.

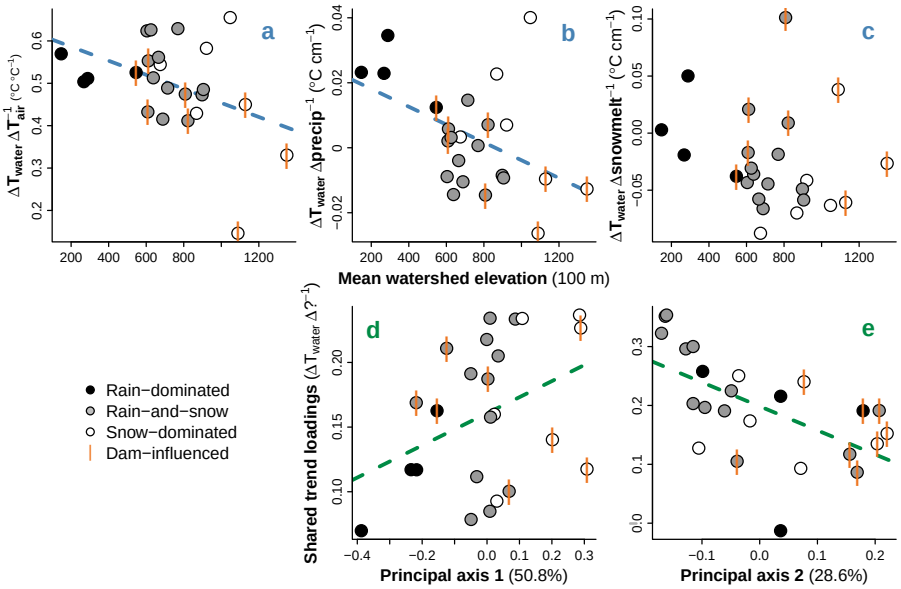
a
b
c
d
e
Mean watershed elevation (100 m)
Rain−dominated
Rain−and−snow
Snow−dominated
Dam−influenced
Principal axis 1 (50.8%)
Principal axis 2 (28.6%)

254

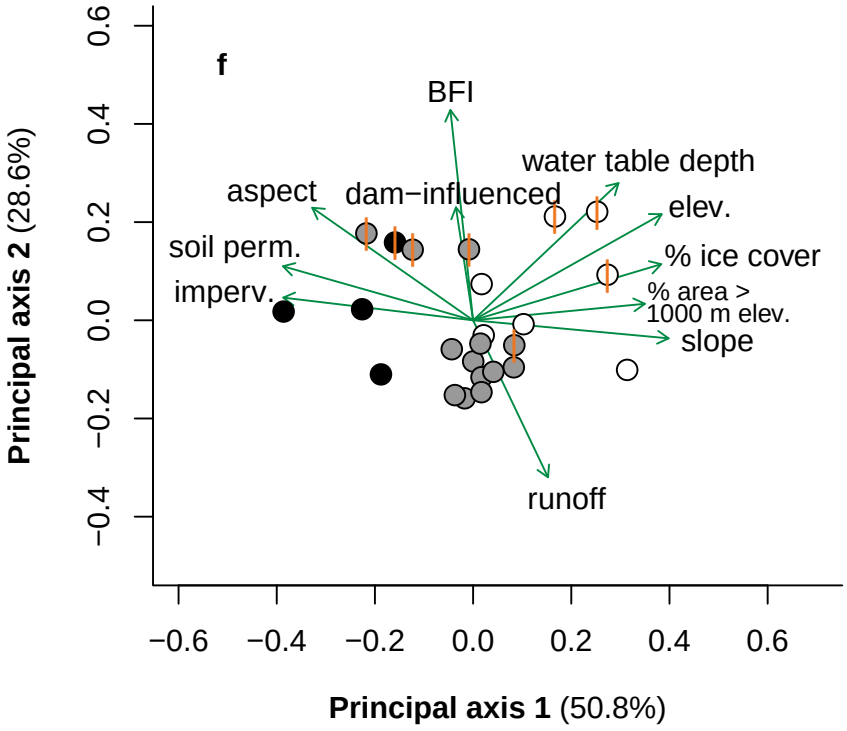

255

256 **Figure 3** (a-c) Relationships between watershed elevation and climatic effects
257 on T_{water}, and (d-e) between watershed features and factor loadings on shared
258 trends. Regression lines indicate slopes significant at $\alpha = 0.1$. (f) Ordination of
259 landscape predictors by principal coordinates analysis. Length and direction of
260 arrows are proportional to loading of landscape predictors onto each principal
261 axis of their variation.

262

263 DFA results, aggregated across months and years for each site, revealed a
264 trend toward reduced $T_{air} \rightarrow T_{water}$ coupling with increasing watershed ele-
265 vation ($p = 0.04, R^2 = 0.18$; Fig. 3a). On average, a 1°C change in T_{air}
266 corresponded to a 0.53 ± 0.03°C change in T_{water} at RD, a 0.51 ± 0.08°C change
267 at RS, and a 0.45 ± 0.17°C change at SD sites. A similar trend was observed
268 with respect to $precip \rightarrow T_{water}$ coupling ($p = 0.03, R^2 = 0.21$; Fig. 3b), where
269 a monthly change in total precipitation of 1 cm corresponded to a 0.02 ± 0.009°C
270 change in T_{water} for RD, -0.003 ± 0.009°C for RS, and 0.004 ± 0.02°C for SD.

There was no evidence of coupling between snowmelt and T_{water} (Fig. 3c), but this predictor was included in the most parsimonious DFA model selected via AIC and R^2 (See Appendix A.). It is of note that the strongest examples of $T_{air} \rightarrow T_{water}$ and $precip \rightarrow T_{water}$ coupling were observed in the Duckabush River, while the weakest examples are from the Elwha River. Both rivers drain glaciers of the Olympic Mountain Range, and both are SD, though the Elwha's watershed is larger.

In addition to the three climate predictors above, the best T_{water} model also included five shared trends. Of these, four correlated significantly with at least one known watershed predictor. Figure 3 depicts the strongest correlated variables with each trend (insets d-e). These are, in arbitrary order of relevance, mean water table depth ($p < 0.001, R^2 = 0.60$; Fig. 3d), % glaciation ($p < 0.01, R^2 = 0.30$; Fig. 3e), BFI ($p = 0.01, R^2 = 0.25$; Fig. 3f), and mean slope ($p < 0.01, R^2 = 0.29$; Fig. 3g). The fifth shared trend was not correlated with any variables in the watershed predictor dataset.

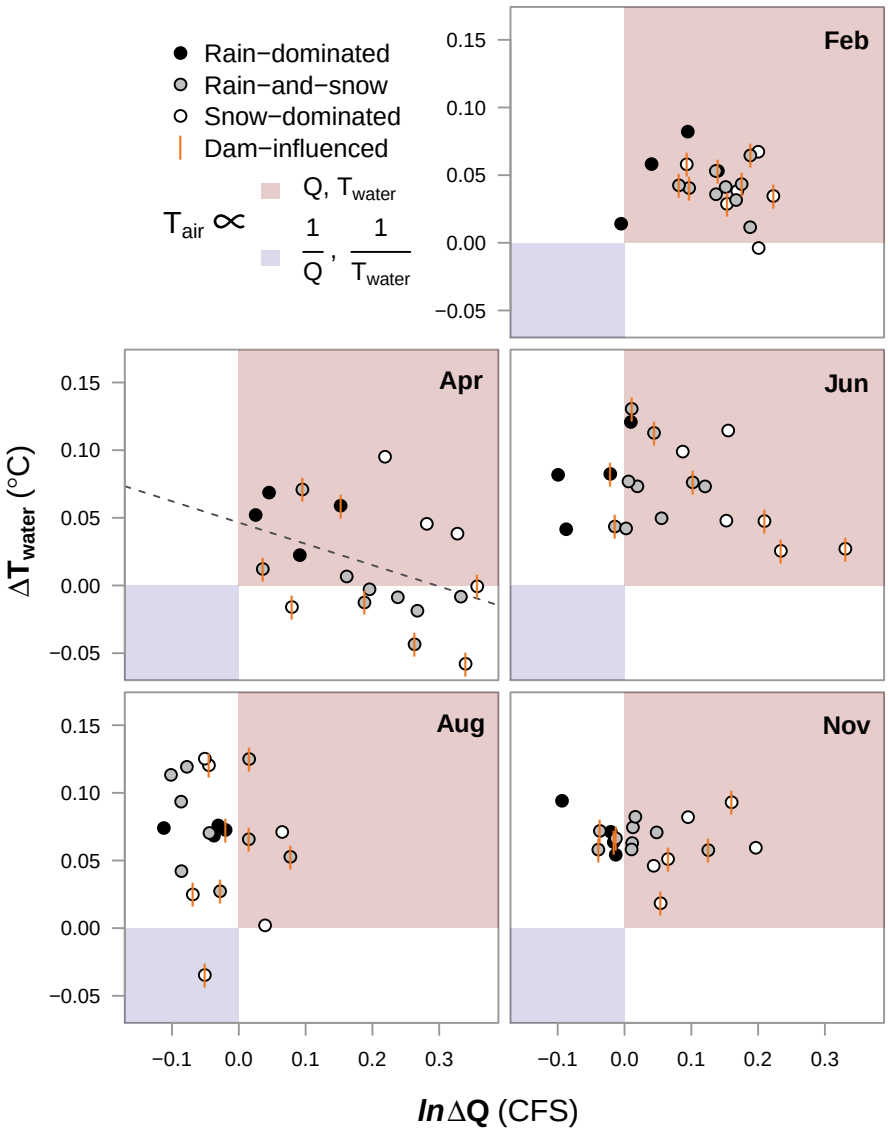

Figure 4 Relationship between $T_{air} \rightarrow T_{water}$ and $T_{air} \rightarrow Q$. Both axes are expressed per 1°C change in T_{air}. The red quadrant designates proportionality between all three variables, the blue inverse proportionality between each response and T_{air}. Regression lines indicate slopes significant at $\alpha = 0.05$.

To examine possible sub-season interactions between T_{air}, T_{water} and Q, we performed an additional DFA with Q as the response. In both models, T_{air} was

allowed to have unique monthly effects. These effects, taken together, can be understood in relation to the four quadrants of the Cartesian coordinate system (increasing clockwise from upper right; Fig. 4).

In mid-winter (exemplified by February), all river classes primarily occupy the first quadrant, signifying $T_{\text{air}} \propto T_{\text{water}}$ and $T_{\text{air}} \propto Q$, where $\propto$ denotes proportionality. RD shows the weakest Q response. By spring, many RS and SD sites develop an inverse relationship between T_{air} and T_{water}, denoted $T_{\text{air}} \propto \frac{1}{T_{\text{water}}}$, while RD sites change little from their winter state. June and August see a procession of most sites into the near fourth quadrant, with SD trailing. This signifies $T_{\text{air}} \propto \frac{1}{Q}$, though $T_{\text{air}} \propto T_{\text{water}}$ remains. One stark exception is again the Elwha river, which occupies quadrant three. By fall, RS and SD have begun progress back toward their winter states, led by SD. RD, meanwhile, remain essentially unmoved from summer.

Discussion

The effects of climate on T_{water}, determined by dynamic factor analysis, suggest that nearly all rivers included in our dataset were influenced strongly by air temperature, precipitation, and/or snowmelt across 38 years of monthly data (Fig. 3). At most monitoring sites, T_{water} closely tracked changes in T_{air}, on average responding to increases and decreases with proportional movements of up to 66% magnitude. However, some rivers only weakly track T_{air}, and several patterns in the intensity of this coupling correlate strongly with watershed features relating to ice, groundwater, and slope. Glaciation and yearly snow burden are prominent among these, and for reasons of ecological and hydrological implication, the primary focus of the following discussion.

Without any analysis, a "buffering" effect (hereinafter contrasted with "coupling") of ice on river temperature can be seen in the yearly patterns of $_{\text{water}}$ relative to T_{air} (Fig. 2). The aggregate hydrograph peaks due to snowmelt from April to June, at the same time that the trajectories of RS and SD (snow-influenced rivers) start to drop off relative to RD. After snowmelt begins to subside, RS and SD recover with a noticeable jump. For rivers that receive glacial runoff (SD), this effect appears to remain, buffering them from summer temperature rise where RS rivers instead take on the character of RD (Fig. 4). In an extreme case, the Elwha River was actually cooler in August during those years in which air temperature was higher, likely due to increased runoff from Carrie and Eel glaciers. The buffering effect of ice on river temperature is therefore two-fold, acting first on all snowmelt-influenced rivers through a cold-water pulse in spring, and then on a subset of those rivers throughout summer and fall, by way of glacial runoff. For RD rivers, which receive little to no input from ice, summer temperature is entirely dictated by that of the surrounding air, and whatever rain falls through it. Though higher-elevation watersheds will always produce colder water, independent of the influence of ice, it can be expected that RS and SD rivers will grow more similar to RD as regional temperatures warm and glaciers decline. That is to say, formerly reliably cold-water

streams and associated habitats may see increases in both summer and winter average temperatures, as well as higher variability from year to year. The Elwha in particular may slip from its current state of high resistance to seasonal climatic changes. We tested for changes in mean and variance of $T_{\text{air}} \rightarrow T_{\text{water}}$ and $T_{\text{air}} \rightarrow Q$ coupling between 1978 and 2015, but did not detect any regular patterns (Appendix B).

In addition to the three climate predictors, five shared trends were fit by the most parsimonious DFA model. These represent additional drivers responsible for structuring water temperature across some or all of the 24 sites included in the analysis. Each monitoring sites' factor loading on a particular shared trend indicates the degree to which the trend accounted for variance in T_{water} at that site. While the precise identities of these drivers cannot be obtained with certainty, they can be inferred through correlation with predictor variables. In this way, we determined the most likely landscape drivers of T_{water} to be perennial ice and snow cover, mean watershed slope, and groundwater influx. In the case of slope, the likely mechanism of influence is increased turbulence and mixing of water and air in steep, headwater streams, which allows convective warming and cooling to occur more rapidly Brutsaert 1975; Fig. 3g). As for groundwater, greater influx (represented by baseflow index, or BFI; fig. 3f) corresponds to greater *de*-coupling of climatic effects and river temperature, as groundwater should be insulated relative to surface water. For the same reason, greater depth of groundwater should be associated with better insulation and thus further decoupling (Fig. 3d). The buffering effect of perennial ice and snow on SD rivers has already been discussed, but the uniquely high factor loadings of RS rivers in relation to the associated trend are worth noting (Fig. 3e). This trend may account for variation in RS due to traits shared by RD and SD, or to a "rain-on-snow" effect that may yield additional cold water in early spring. The fifth trend did not correlate strongly with any of the landscape predictors in our dataset. It may therefore represent additional, unknown drivers like marine or microclimatic effects, or it may simply account for random noise.

The relationship between climate and river temperature is further influenced by the interaction of discharge, and the fates of rivers in the Puget Sound watershed can be best understood by examining these factors in combination (Fig. 4). Whether rain-, both-, or snow-dominated, all rivers took on RD characteristics in winter, when the effects of ice lay latent. As a result, warmer Februaries on average yielded warmer rivers and higher flow (less precipitation bound in ice). The critical differences between river classes played out in spring and summer, and it's during these months that future purturbations due to changing climate may be felt most acutely. For example, warmer Aprils on average produced colder water at 9 out of 15 RS and SD sites. Though we determined discharge, groundwater, and slope to be likely components of this relationship, only melting ice could be credited with actually reversing it. Projected reductions in snowpack for the Pacific Northwest can therefore be expected to fundamentally alter the responses of currently snow-influenced rivers to yearly variation in spring temperature. In the longer term, changes can be expected for rivers that now receive the temperature-buffering effect of glacial runoff. Glaciers continue to

decline across North America, with glacial ice across Western Canada projected to decline by 70% from 2005 to 2100 (Clarke et al., 2015).

Conclusion

Temperature regimes across the rivers of the Puget Sound watershed are structured by a combination of climatic drivers at the regional scale, and geophysical drivers at watershed scales. In the absence of snow and ice, river temperature is closely coupled to that of the surrounding air, while contributions of snowmelt and glacial runoff can dampen or even reverse this coupling in spring and summer. In some cases, icemelt-influenced rivers exhibit stronger positive responses to climate patterns than their rain-driven counterparts. Our results suggest elevational variations in groundwater influx, total discharge, and watershed slope account for these patterns. However, while these factors may influence the degree of coupling between climatic drivers and water temperature, only snow and ice can reverse it. Since 1978, such reversals have been widespread, particularly during spring melt. Though we did not detect changes in this effect across historical observations, future reductions in snowpack and glacial mass are projected. Consequently, many rivers that now undergo the mildest seasonal temperature changes may be impacted most strongly.

References

ArcMap (2016). Environmental systems research institute (esri). *Redlands, CA: http://www.esri.com/*.

Boisneau, C., Moatar, F., Bodin, M., and Boisneau, P. (2008). *Does global warming impact on migration patterns and recruitment of Allis shad (Alosa alosa L.) young of the year in the Loire River, France?*, pages 179–186. Springer Netherlands, Dordrecht.

Boscarino, B. T., Rudstam, L. G., Mata, S., Gal, G., Johannsson, O. E., and Mills, E. L. (2007). The effects of temperature and predatorprey interactions on the migration behavior and vertical distribution of mysis relicta. *Limnology and Oceanography*, 52(4):1599–1613.

Brutsaert, W. (1975). A theory for local evaporation (or heat transfer) from rough and smooth surfaces at ground level. *Water resources research*, 11(4):543–550.

Burnham, K. P. and Anderson, D. R. (2003). *Model selection and multimodel inference: a practical information-theoretic approach*. Springer Science & Business Media.

Carter, K. (2005). The effects of temperature on steelhead trout, coho salmon, and chinook salmon biology and function by life stage. *Implications for the Klamath River total maximum daily loads. California Regional Water Quality Control Board. North Coast Region, Santa Rosa, California*.

Clarke, G. K., Jarosch, A. H., Anslow, F. S., Radić, V., and Menounos, B. (2015). Projected deglaciation of western canada in the twenty-first century. *Nature Geoscience*, 8(5):372–377.

Eldridge, E. (1967). Water temperature: influences, effects, and control. Technical report, Federal Water Pollution Control Administration, Portland, Oreg.(USA). Northwest Region.

Garner, G., Hannah, D. M., Sadler, J. P., and Orr, H. G. (2014). River temperature regimes of england and wales: spatial patterns, inter-annual variability and climatic sensitivity. *Hydrological Processes*, 28(22):5583–5598.

Gower, J. C. (1966). Some distance properties of latent root and vector methods used in multivariate analysis. *Biometrika*, 53(3/4):325–338.

Harvey, A. C. (1990). *Forecasting, structural time series models and the Kalman filter*. Cambridge university press.

Hill, R. A., Weber, M. H., Leibowitz, S. G., Olsen, A. R., and Thornbrugh, D. J. (2016). The stream-catchment (streamcat) dataset: A database of watershed metrics for the conterminous united states. *JAWRA Journal of the American Water Resources Association*, 52(1):120–128.

Holmes, E. E., Ward, E. J., and Wills, K. (2012). Marss: Multivariate autoregressive state-space models for analyzing time-series data. *The R Journal*, 4(1):11–19.

Kristensen, K., Nielsen, A., Berg, C. W., Skaug, H., and Bell, B. (2015). Tmb: automatic differentiation and laplace approximation. *arXiv preprint arXiv:1509.00660*.

Kristensen, K., Nielsen, A., Berg, C. W., Skaug, H., and Bell, B. M. (2016). TMB: Automatic differentiation and Laplace approximation. *Journal of Statistical Software*, 70(5):1–21.

Lisi, P. J., Schindler, D. E., Bentley, K. T., and Pess, G. R. (2013). Association between geomorphic attributes of watersheds, water temperature, and salmon spawn timing in alaskan streams. *Geomorphology*, 185:78–86.

Lisi, P. J., Schindler, D. E., Cline, T. J., Scheuerell, M. D., and Walsh, P. B. (2015). Watershed geomorphology and snowmelt control stream thermal sensitivity to air temperature. *Geophysical Research Letters*, 42(9):3380–3388.

Mauger, G., Casola, J., Morgan, H., Strauch, R., Jones, B., Curry, B., Isaksen Busch, T., et al. (2015). State of knowledge: Climate change in puget sound.

McCullough, D. A. (1999). *A review and synthesis of effects of alterations to the water temperature regime on freshwater life stages of salmonids, with special reference to Chinook salmon*. US Environmental Protection Agency, Region 10.

McKay, L., Bondelid, T., Dewald, T., Johnston, J., Moore, R., and Rea, A. (2012). Nhdplus version 2: user guide. *National Operational Hydrologic Remote Sensing Center, Washington, DC*.

Mote, P. W. and Salathe, E. P. (2010). Future climate in the pacific northwest. *Climatic Change*, 102(1-2):29–50.

NOAA (2017). National centers for environmental information, climate at a glance: U.s. time series. Data retrieved from: `http://www.ncdc.noaa.gov/cag/` on 11/10/2016.

Poole, G. C. and Berman, C. H. (2001). An ecological perspective on in-stream temperature: natural heat dynamics and mechanisms of human-causedthermal degradation. *Environmental management*, 27(6):787–802.

R Core Team (2017). *R: A Language and Environment for Statistical Computing*. R Foundation for Statistical Computing, Vienna, Austria.

Radeloff, V. C., Nelson, E., Plantinga, A. J., Lewis, D. J., Helmers, D., Lawler, J., Withey, J., Beaudry, F., Martinuzzi, S., Butsic, V., et al. (2012). Economic-based projections of future land use in the conterminous united

states under alternative policy scenarios. *Ecological Applications*, 22(3):1036–1049.

Reidy Liermann, C., Olden, J. D., Beechie, T., Kennard, M. J., Skidmore, P., Konrad, C., and Imaki, H. (2012). Hydrogeomorphic classification of washington state rivers to support emerging environmental flow management strategies. *River Research and Applications*, 28(9):1340–1358.

USDA (2017). National resources conservation service. Data retrieved from: `https://www.nrcs.usda.gov/wps/portal/nrcs/detail/or/snow/?cid=nrcs142p2_046350` on 1/23/2017.

USGS (2017). National water information system. Data retrieved from: `http://www.ecy.wa.gov/programs/eap/fw_riv/index.html` on 1/30/2017.

van Vliet, M. T., Franssen, W. H., Yearsley, J. R., Ludwig, F., Haddeland, I., Lettenmaier, D. P., and Kabat, P. (2013). Global river discharge and water temperature under climate change. *Global Environmental Change*, 23(2):450–464.

Von Prause, M. (2017). River and stream water quality monitoring program. Data retrieved from Washington Department of Ecology: `http://www.ecy.wa.gov/programs/eap/fw_riv/index.html` on 7/1/2016.

Ward, J. (1985). Thermal characteristics of running waters. In *Perspectives in Southern Hemisphere Limnology*, pages 31–46. Springer.

Zuur, A., Tuck, I., and Bailey, N. (2003a). Dynamic factor analysis to estimate common trends in fisheries time series. *Canadian journal of fisheries and aquatic sciences*, 60(5):542–552.

Zuur, A. F., Fryer, R., Jolliffe, I., Dekker, R., and Beukema, J. (2003b). Estimating common trends in multivariate time series using dynamic factor analysis. *Environmetrics*, 14(7):665–685.

Appendix A

Temperature DFA output and diagnostics

Model selection included four climate covariates (air temperature, precipitation, snowmelt, and hydrological drought), between 1 and 15 shared trends, four within-and-among-site error structures (see methods), and two models of unknown seasonal variation (fixed monthly factors and Fourier series). The most parsimonious model of river temperature was selected using the Akaike Information Criterion (AIC), and included air temperature, precipitation, and snowmelt as covariates. This model also included five shared trends and an independent and unequally distributed error structure among streams (i.e. diagonal and unequal variance-covariance matrix).

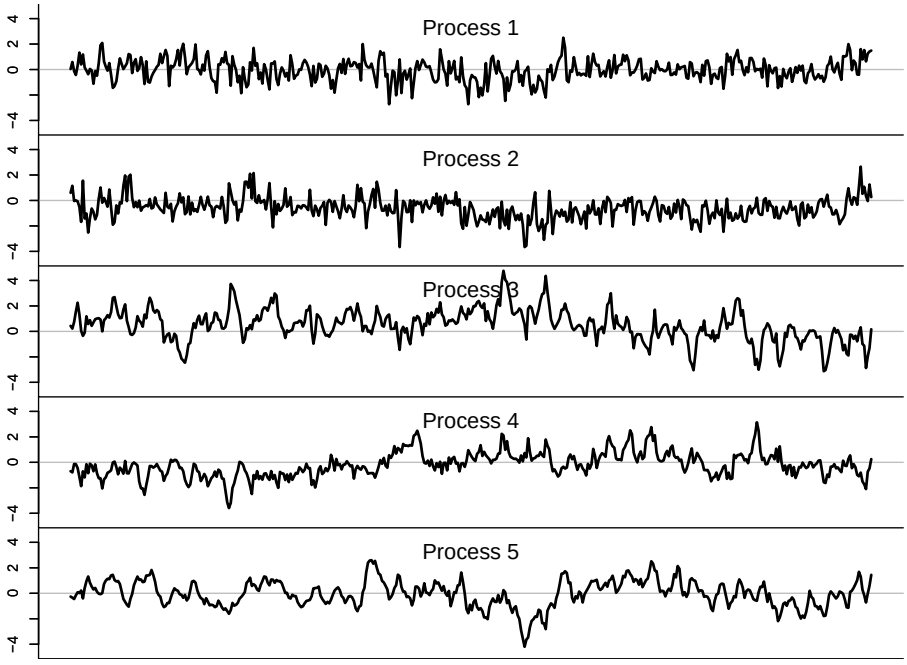

Figure A1 Shared trends.

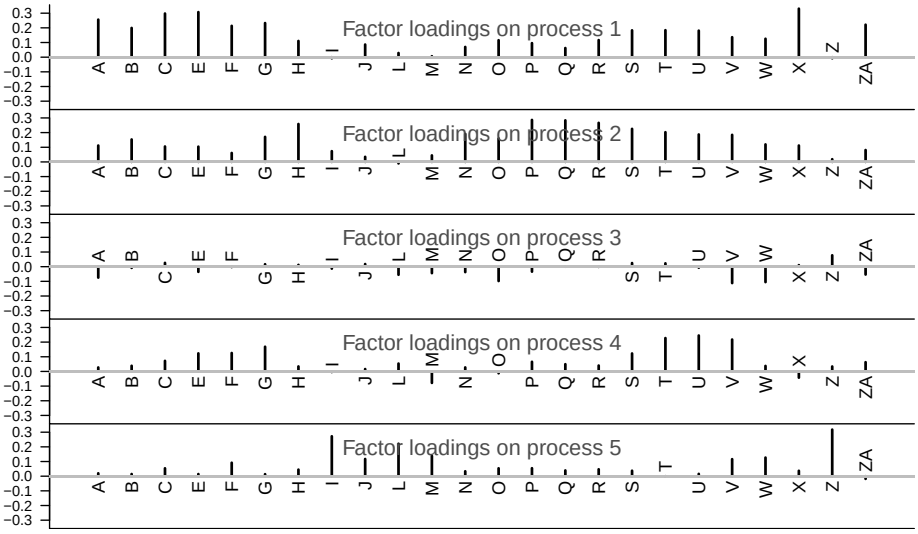

Figure A2 Factor loadings on shared trends.

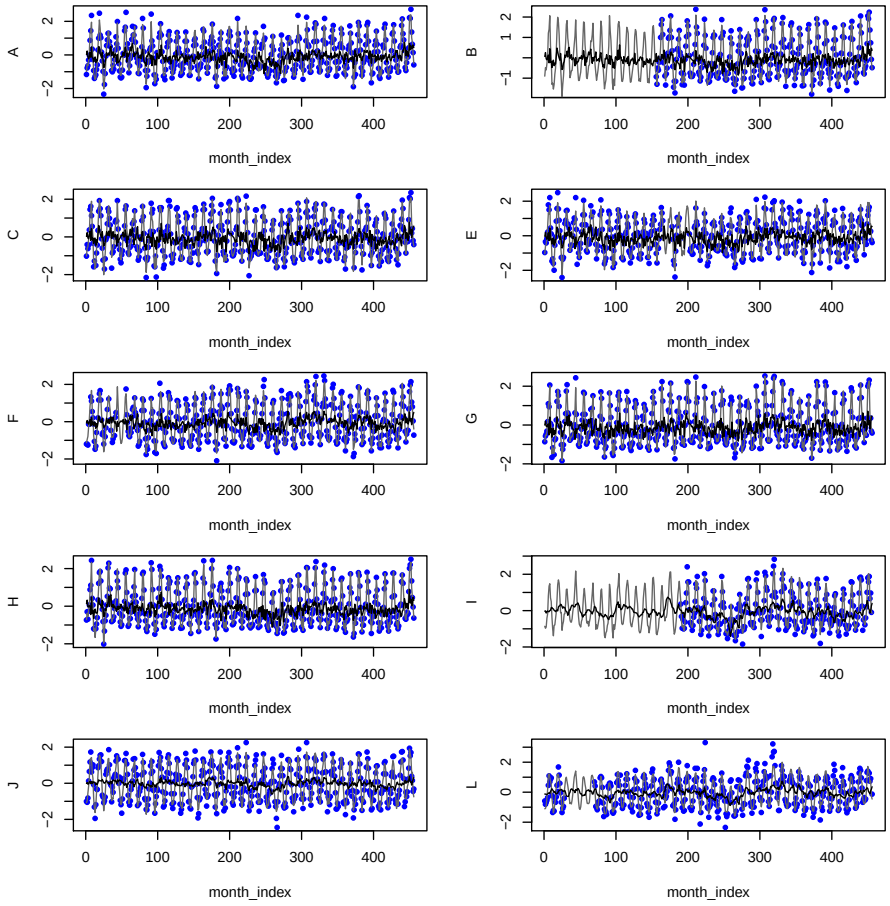

Figure A3 Model fits (gray line = overall; black line = trends-only).

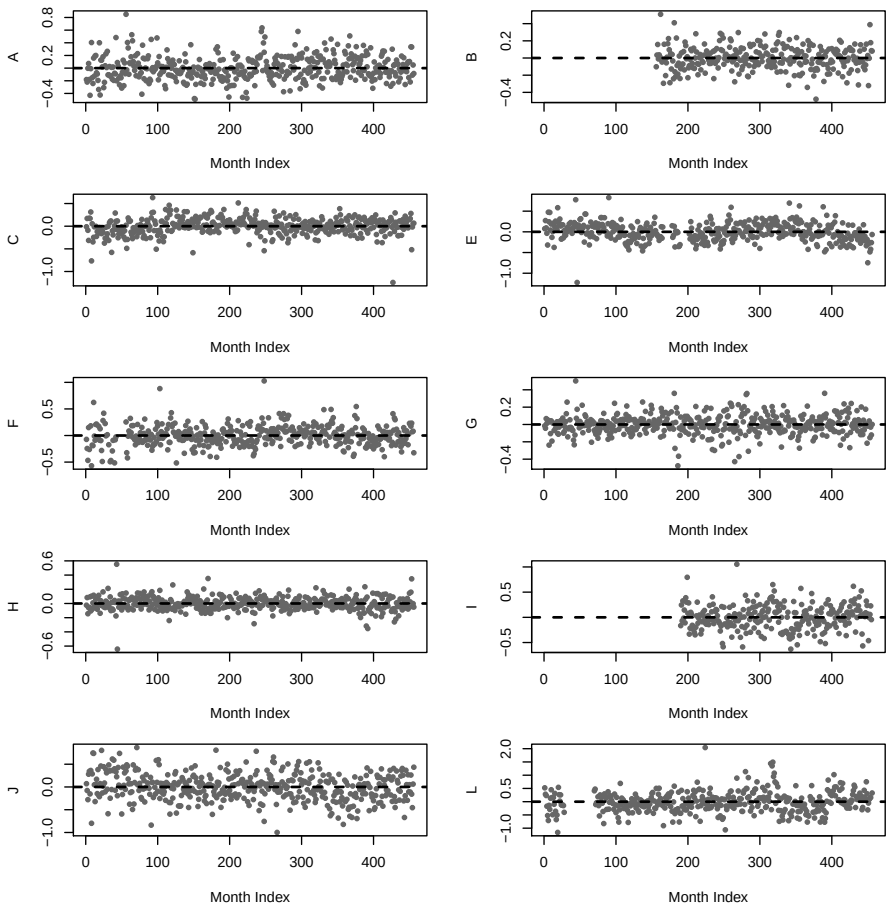

Figure A4 Residuals.

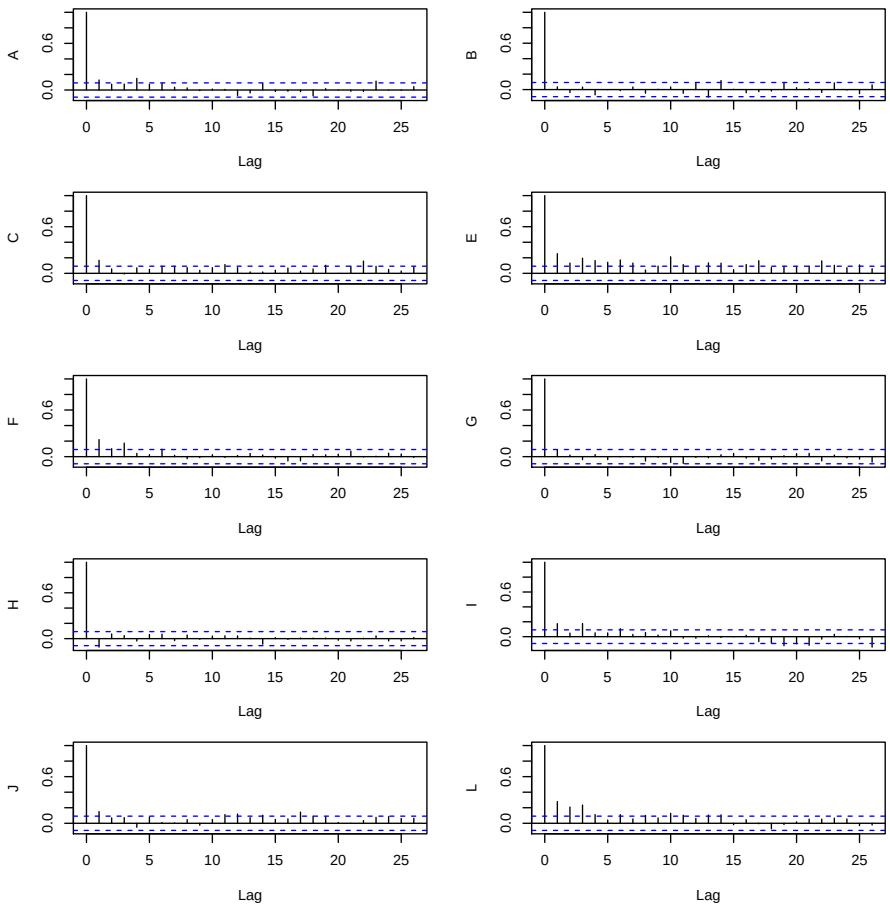

Figure A5 Autocovariance function (ACF).

Output from the discharge model looks very similar to this, and is omitted here for the sake of retaining a reasonable page count.

Appendix B

Testing for change in coupling over time

We used an additional DFA model to test for changes in $T_{air} \rightarrow T_{water}$ coupling over time, by dividing the 1978-2015 time series into 5 intervals and comparing central tendency and variance of effect sizes for each interval. Figures B1-B3 show mean effect size for each stream.

To approximate estimates of variability over time, we performed the same analysis within a Bayesian framework, and obtained uncertainty estimates from the credible intervals of the effect size posteriors. This approach yielded no trends in variation over time, and is not visualized here (This will be included in the final version of this paper).

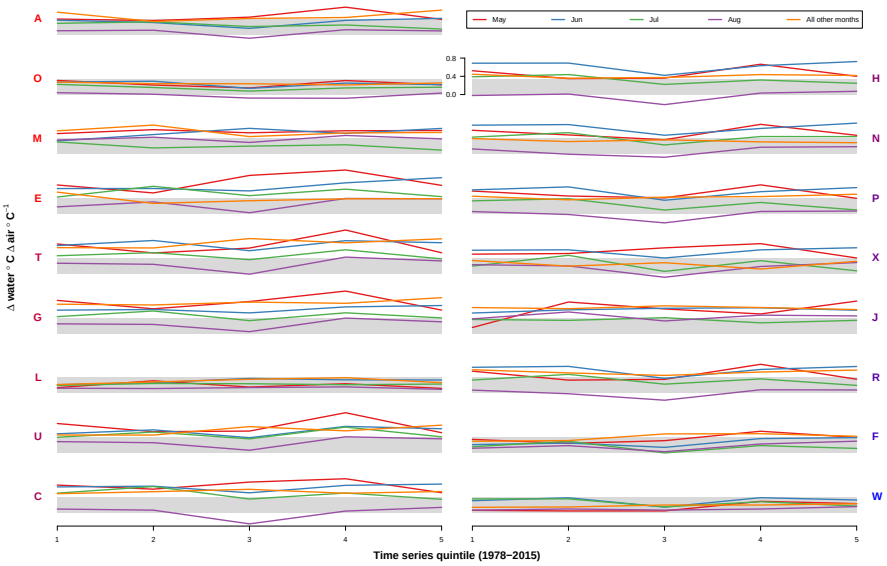

Figure B1 Mean $T_{air} \rightarrow T_{water}$ coupling over time. Each plot corresponds to an individual site. Y-label colors represent mean watershed elevation (bluer=higher).

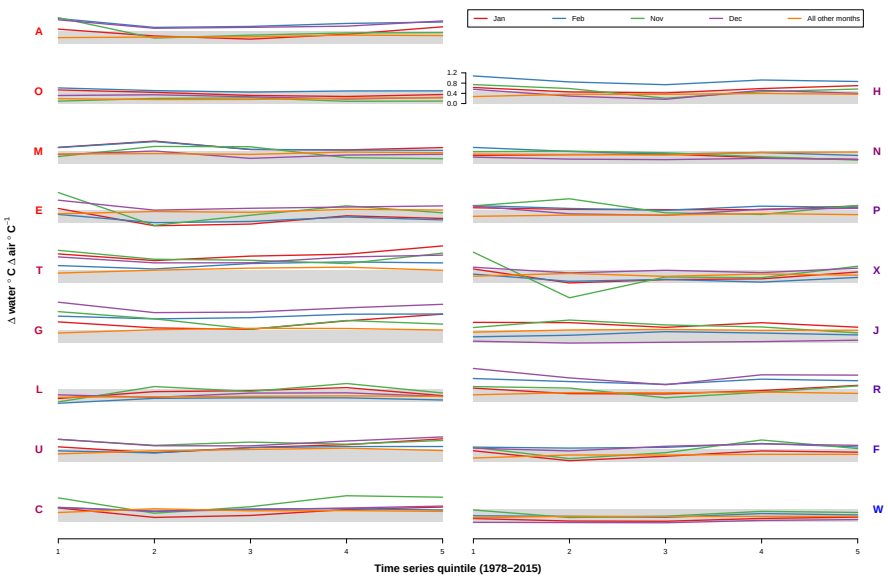

Figure B2 Mean $T_{air} \rightarrow T_{water}$ coupling over time. Each plot corresponds to an individual site. Y-label colors represent mean watershed elevation (bluer=higher).

Figure B3 Mean $T_{air} \rightarrow T_{water}$ coupling over time. Each plot corresponds to an individual site. Y-label colors represent mean watershed elevation (bluer=higher).